Tensor Oriented No-Reference Light Field Image Quality Assessment

Wei Zhou, Likun Shi, and Zhibo Chen, *Senior Member, IEEE*

Abstract—Light field image (LFI) quality assessment is becoming more and more important, which helps to better guide the acquisition, processing and application of immersive media. However, due to the inherent high dimensional characteristics of LFI, the LFI quality assessment turns into a multi-dimensional problem that requires consideration of the quality degradation in both spatial and angular dimensions. Therefore, we propose a novel Tensor oriented No-reference Light Field image Quality evaluator (Tensor-NLFQ) based on tensor theory. Specifically, since the LFI is regarded as a low-rank 4D tensor, the principle components of four oriented sub-aperture view stacks are obtained via Tucker decomposition. Then, the Principal Component Spatial Characteristic (PCSC) is designed to measure the spatial-dimensional quality of LFI considering its global naturalness and local frequency properties. Finally, the Tensor Angular Variation Index (TAVI) is proposed to measure angular consistency quality by analyzing the structural similarity distribution between the first principal component and each view in the view stack. Extensive experimental results on four publicly available LFI quality databases demonstrate that the proposed Tensor-NLFQ model outperforms state-of-the-art 2D, 3D, multi-view, and LFI quality assessment algorithms.

Index Terms—Light field, image quality assessment, objective model, tensor theory, angular consistency.

I. INTRODUCTION

AS an important medium for human visual perception, light enables humans to effectively perceive the spatial, color, form and dynamic changes of our environment. Conventional media modalities such as 2D images mainly consider the intensity information of radiance, which can only provide a two-dimensional sense of presence. Different from traditional image capturing formats, light field content records both radiation intensity and direction information of light rays in the free space, thus providing an enhanced immersive experience. Considering the abundant spatial and angular information of the light field, its processing and application have attracted widespread attention in past decades. However, these operations inevitably introduce heterogeneous artifacts, resulting in the degradation of the perceptual quality for light field content [1]. Therefore, monitoring the perceptual quality of light field content is critical to better guiding the procedure of light field acquisition, processing and application techniques.

To facilitate the recording and processing of light field content, a 4D function based on the assumption that the light ray radiance is monochromatic, time-invariant and constant

The authors are with the CAS Key Laboratory of Technology in Geo-Spatial Information Processing and Application System, University of Science and Technology of China, Hefei 230027, China (e-mail: weichou@mail.ustc.edu.cn; : slikun@mail.ustc.edu.cn; chenzhibo@ustc.edu.cn).

Wei Zhou and Likun Shi contributed equally to this paper.

along a straight line is adopted to represent light field data [2], [3]. Specifically, light field is parameterized by four coordinates $\mathbf{L}(s,t,x,y)$, where the s,t dimensions are angular dimensions and x,y dimensions denote spatial dimensions. When a 4D light field image (LFI) is captured by Lytro Illum [4], each view in the LFI is called a sub-aperture image (SAI). Due to the high dimensional characteristics of LFI, its quality is influenced by different dimension of impairments than that of traditional media. Therefore, it is necessary to analyze the specific factors in LFI quality assessment. The existing research works based on subjective evaluation [5]–[9] found that the LFI quality assessment needs to consider from these three aspects, namely spatio-angular resolution, spatial quality, and angular consistency. Specifically, spatio-angular resolution refers to the number of SAIs in a LFI and the resolution of a SAI. Spatial quality indicates the quality of SAIs and angular consistency measures the visual coherence between SAIs. Since the spatio-angular resolution is usually determined by the acquisition devices, this paper focuses on the effects of spatial quality and angular consistency.

Although subjective evaluation is an effective way to understand human behavior and provides reliable image quality scores, it is resource and time consuming without the possibility to be applied for practical applications. Therefore, an effective objective LFI quality assessment model is necessary. Conventionally, image quality assessment (IQA) models can be roughly classified into three categories based on the availability of original reference image information: full-reference (FR), reduced-reference (RR) and no-reference (NR).

Specifically, FR IQA approaches utilize the complete reference image information and measure the difference between reference and distorted images. Among a variety of 2D FR IQA methods, structure similarity between reference and distorted images is measured in structural similarity (SSIM) [10], and several of its variants have been proposed, i.e. multi-scale SSIM (MS-SSIM) [11], feature similarity (FSIM) [12], information content weighted SSIM (IW-SSIM) [13], and so on [14]–[16]. The information fidelity criterion (IFC) [17] and visual information fidelity (VIF) [18] measure the degree of information loss of the distorted images relative to the reference image. Moreover, the noise quality measure (NQM) [19] and visual signal-to-noise ratio (VSNR) [20] consider the sensitivity of the human visual system (HVS) to different visual signals. Chen *et al.* [21] proposed a 3D FR IQA algorithm that models the influence of binocular rivalry. For multi-view FR IQA, morphological pyramid decomposition and morphological wavelet decomposition are employed in morphological wavelet peak signal-to-noise ratio (MW-PSNR) [22] and morphological pyramid PSNR (MP-PSNR) [23], [24],
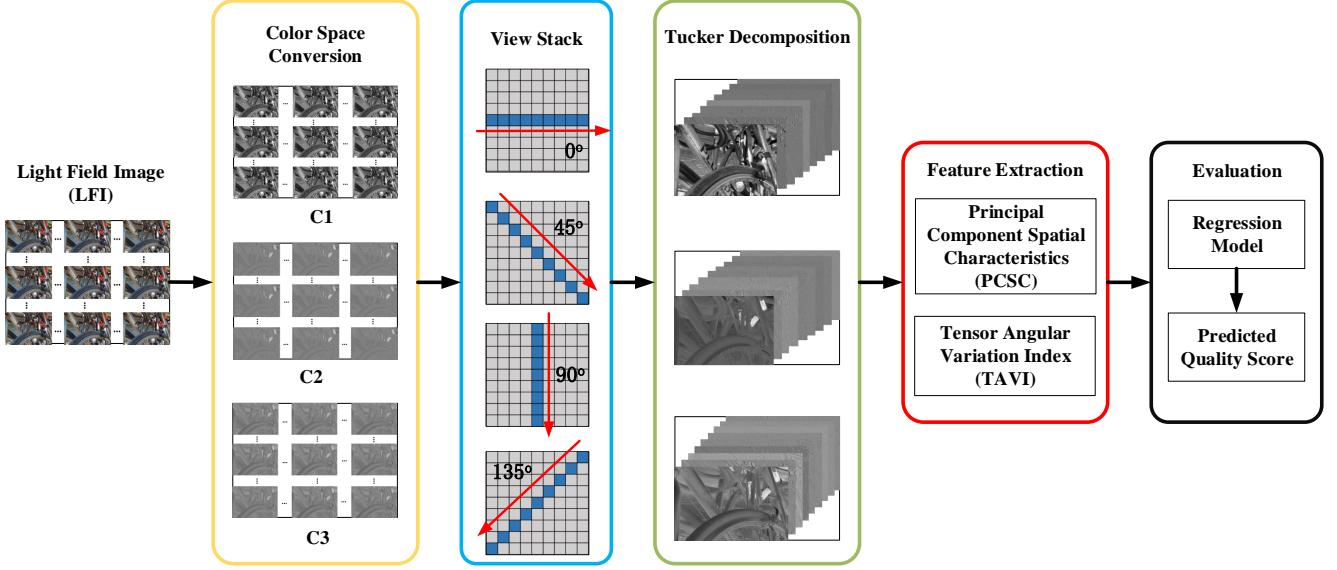
Fig. 1: Flow diagram of the proposed Tensor-NLFQ model.

respectively. The 3D synthesized view image quality metric (3DSwIM) [25] is based on the comparison of statistical features from wavelet subbands.

The RR IQA algorithms utilize partial information of the reference image for quality assessment, which is exploited when the reference information is transmitted at low bandwidth, such as [26]–[28]. The NR IQA methods measure distorted image quality without needing the original image, which is more applicable in most real-world scenarios. For example, natural scene statistics from different domains are extracted to predict 2D image quality [29]–[33]. For 3D NR IQA, binocular vision theory and depth perception are adopted in several methods [34]–[36]. Gu *et al.* [37] proposed a multi-view NR IQA algorithm named autoregression (AR)-plus thresholding (APT) that employs the AR-based local image description. However, none of the aforementioned schemes consider the intrinsic high dimensional characteristics of LFI, especially the distortion caused by angular consistency. Therefore, it is important and necessary to design a new light-field-specific metric.

In the literature, several LFI quality assessment models have been proposed. Fang *et al.* [38] proposed a FR LFI quality assessment method that measures the gradient magnitude similarity of reference and distorted epipolar plane images. Huang *et al.* [39] also proposed a FR LFI quality assessment algorithm, which is based on dense distortion curve analysis and scene information statistics. The light field image quality assessment metric (LF-IQM) [40] is a RR LFI quality assessment metric that assumes the depth map quality is closely related to the LFI overall quality and measures the structural similarity between original and distorted depth maps to predict the perceived LFI quality. However, Fang [38] and LF-IQM [40] ignore the texture information of SAI, which result in the insufficient measurement of the LFI spatial quality. Furthermore, the performance of the LF-

IQM is significantly affected by the adopted depth estimation algorithms. Additionally, in most cases, the pristine image is not available, thus NR LFI quality assessment methods are desired. To the best of our knowledge, our previous work [41] propose the only NR LFI quality assessment metric called blind quality evaluator of light field image (BELIF), which utilizes binocular vision features for measuring the spatial quality and angular consistency.

However, most of them ignore the intrinsic high dimensional characteristics of LFI. In recent works, the tensor theory has been successfully applied to many fields of computer vision, such as compression and recognition [42]. Mathematically, a LFI belongs to a 4D tensor. Therefore, the tensor theory can effectively describe the characteristics and distributions in the high-dimensional space. Moreover, these aforementioned methods are designed to extract features in the luminance domain. Although luminance is considered as a dominant factor for understanding the human visual perception [43], luminance-based IQA methods may be sub-optimal because they underestimate visual interference caused by color distortion, especially the significant differences in the colors of different SAIs. In addition, existing methods neglect the impact of angular consistency in diverse orientations [40], [41] or only consider horizontal angular consistency [38], [39]. Since the LFI is an image array, the relationship between each SAI and the adjacent SAI can reflect the LFI angular consistency. Generally, a SAI has eight adjacent SAIs that correspond to angular consistency in four orientation, namely horizontal, vertical, left diagonal, and right diagonal orientations.

In this paper, based on the tensor theory, we proposed a novel Tensor oriented No-reference Light Field image Quality evaluator (Tensor-NLFQ), which considers both luminance and chrominance effects, as well as the impact of angular consistency in diverse directions on the LFI quality. Specifically, the SAIs in RGB are first converted into CIELAB color space,
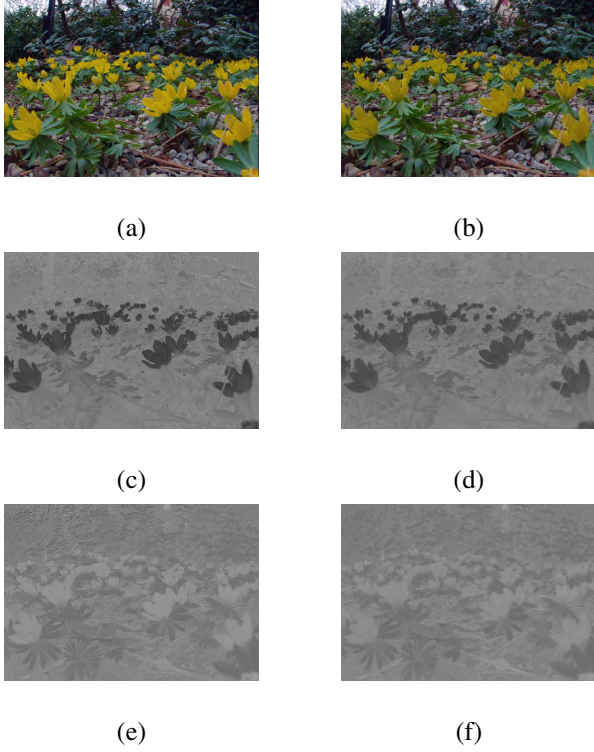
(a)　　　　　　　(b)

(c)　　　　　　　(d)

(e)　　　　　　　(f)

Fig. 2: (a-b) Two horizontal adjacent distorted SAIs from Win5-LID database [8]; (c-d) The corresponding chrominance a^* of (a-b); (e-f) The corresponding chrominance b^* of (a-b).

which contains one luminance and two chrominance channels. Second, to comprehensively capture the degradation of LFI angular consistency, view stacks are generated along four orientations. Third, the Tucker decomposition is employed to reduce the angular dimensional of view stacks and obtain the first principal component as the most important dimensionality reduced image. Fourth, considering that the LFI quality is affected by both the spatial quality and angular consistency, we propose the Principal Component Spatial Characteristics (PCSC) for measuring the spatial quality including two key aspects: i) the naturalness distribution of individual and mutual color channels is extracted to measure the global distortion; ii) local frequency distribution is used to capture local spatial quality degradation. In addition, we propose the Tensor Angular Variation Index (TAVI) to measure the angular consistency, which is computed by analyzing the structural similarity distribution between the first principal component and each view in the view stack. Our experimental results show that the performance of our proposed model correlates well with human visual perception and achieves the state-of-the-art performance. The source codes of Tensor-NLFQ will be available online for public research usage [1].

The remainder of this paper is organized as follows. Section II introduces the details of the proposed model. We then illustrate the experimental results in Section III. Finally, section IV concludes our paper.

[1] http://staff.ustc.edu.cn/~chenzhibo/resource.html

II. PROPOSED METHOD

The framework of Tensor-NLFQ algorithm is illustrated in Fig. 1. First, we convert SAIs in RGB into CIELAB color space. Second, we exploit Tucker decomposition along angular dimension to generate the principal components of view stacks in diverse orientations. Third, the PCSC and TAVI are extracted to measure the degradation of spatial quality and angular consistency, respectively. Finally, we utilize the regression model to predict the perceptual LFI quality.

A. Color Space Conversion

As an important and dense natural visual cue, color information helps the human brain to achieve both low-level and high-level visual perception. Extensive research works have been conducted towards understanding the effects of luminance and chrominance on image quality [33], [44]–[46]. These works prove that the chrominance information has a promising gain for image quality evaluation. Therefore, it is reasonable to use the color space information to evaluate LFI spatial quality. Furthermore, in our previous work [8], we have found that if there exists a significant difference in the color of different SAIs, this may destroy LFI angular consistency. Fig. 2 shows two horizontal adjacent SAIs with reconstruction artifacts selected from Win5-LID database [8] and the corresponding two chrominance components. We can see that there exist color differences in the SAIs and the two chrominance components are differentiable, which indicate that color information can measure the deterioration of LFI angular consistency.

To better approximate color perception in the HVS, the color SAIs of each LFI are transformed into the perceptually relevant CIELAB color space with one luminance (L^*) and two chrominance (a^* and b^*) channels optimized for quantifying perceptual color difference and more compatible with human perception [47]. Specifically, the luminance L^* represents color lightness from black to white. Moreover, a^* indicates the position between red/magenta and green, while b^* represents the position between yellow and blue. Therefore, one luminance map array (C_1) and two chrominance map arrays (C_2 and C_3) can be obtained, as shown in the yellow box in Fig. 1. Meanwhile, C_1, C_2 and C_3 have the same spatial resolution and angular resolution as the original LFI.

B. View Stack

In natural, the distribution of light is continuous. However, for practical usage, the LFI is represented as $\mathbf{L}(s, t, x, y)$, where (s, t) indicates the view index and is an integer. Therefore, except for the corner and boundary SAIs, the remaining SAIs have eight adjacent views. Generally, based on the assumption that the angular resolution of LFI is $S \times T$, each SAI has an angular consistency of four orientations, i.e. $0°$, $45°$, $90°$, and $135°$. As shown in the blue box in Fig. 1, these angles represent horizontal ($0°$), left diagonal ($45°$), vertical ($90°$), and right diagonal ($135°$) orientations. We then stack the SAIs along four orientations to generate view stack as follows:
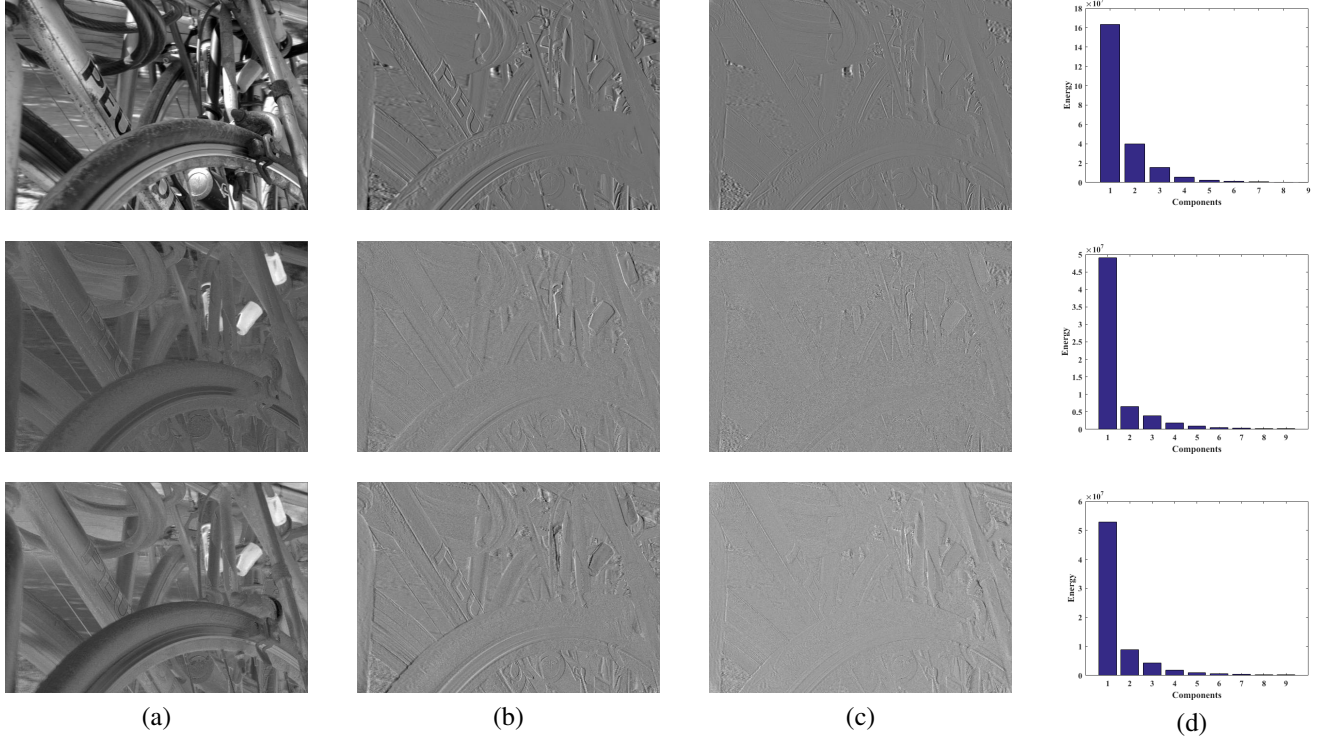
Fig. 3: Tucker decomposition components and their energy histograms. The top, middle and bottom rows denote the components of $\mathscr{C}_1^{0^\circ}$, $\mathscr{C}_2^{0^\circ}$ and $\mathscr{C}_3^{0^\circ}$, respectively. (a) the first principal component; (b) the second principal component; (c) the third principal component; (d) energy distribution of the corresponding decomposition components.

$$C_n^{0^\circ} = \{C_n(s,1,:,:), C_n(s,2,:,:), ..., C_n(s,T,:,:)\}, \quad (1)$$

$$C_n^{90^\circ} = \{C_n(1,t,:,:), C_n(2,t,:,:), ..., C_n(S,t,:,:)\}, \quad (2)$$

$$C_n^{45^\circ} = \{C_n(s,t,:,:), C_n(s+1,t+1,:,:), ...,$$
$$C_n(s+min\{S-s,T-t\}, t+min\{S-s,T-t\},:,:)\}, \quad (3)$$

$$C_n^{135^\circ} = \{C_n(s,t,:,:), C_n(s+1,t-1,:,:), ...,$$
$$C_n(s+min\{S-s,T-1\}, t-min\{S-s,T-1\},:,:)\}, \quad (4)$$

where $s = 1,2,...,S$ and $t = 1,2,...,T$ represent the angular coordinate. $n = 1,2,3$ indicate the luminance and two chrominance channels.

C. Tucker Decomposition

The view stack is a 3D signal that includes two spatial coordinates and one angular coordinate. We discover that there exists a high texture similarity between different images of the view stack, indicating that there exists a large redundancy in the angular dimension. To alleviate this problem, we first adopt tensor decomposition to remove redundant information from the angular dimension, which is equal to the higher-order

principal component analysis (PCA) or singular value decomposition (SVD) [48]. Specifically, the Tucker decomposition is used to achieve dimensionality reduction [42]. It decomposes a tensor into a core tensor multiplied by a matrix along each dimension. For horizontal view stack $C_n^{0^\circ}$, we thus have:

$$C_n^{0^\circ} \approx \mathscr{G} \times_1 U_1 \times_2 U_2 \times_3 U_3, \quad (5)$$

where $\mathscr{G} \in \mathbb{R}^{R_1 \times R_2 \times R_3}$ is the core tensor whose entries illustrate the level of interaction between different components. $U_1 \in \mathbb{R}^{K_1 \times R_1}$ and $U_2 \in \mathbb{R}^{K_2 \times R_2}$ are the factor matrices in the spatial dimension. $U_3 \in \mathbb{R}^{K_3 \times R_3}$ is the angular dimension factor matrix. These matrices are usually orthogonal. In our model, we set $K_n = R_n$, where $n = 1,2,3$.

Then, for $C_n^{0^\circ}$, the angular decomposition components can be obtained by multiplying the core tensor with the factor matrices U_1 and U_2 along each mode in the spatial dimension, which can be given by:

$$\mathscr{C}_n^{0^\circ} = \mathscr{G} \times_1 U_1 \times_2 U_2. \quad (6)$$

Similar to the computation process of $\mathscr{C}_n^{0^\circ}$, we obtain the angular decomposition components $\mathscr{C}_n^{45^\circ}$, $\mathscr{C}_n^{90^\circ}$ and $\mathscr{C}_n^{135^\circ}$ of view stacks in other orientations. Specifically, we utilize the alternating least squares (ALS) method provided by the tensor toolbox [49] to implement the Tucker decomposition.

Fig. 3 (a)-(c) illustrates the first three principal components of $\mathscr{C}_1^{0^\circ}$, $\mathscr{C}_2^{0^\circ}$ and $\mathscr{C}_3^{0^\circ}$. Fig. 3 (d) shows the energy histogram distribution of the corresponding decomposition components. Here, the top, middle and bottom rows denote the components
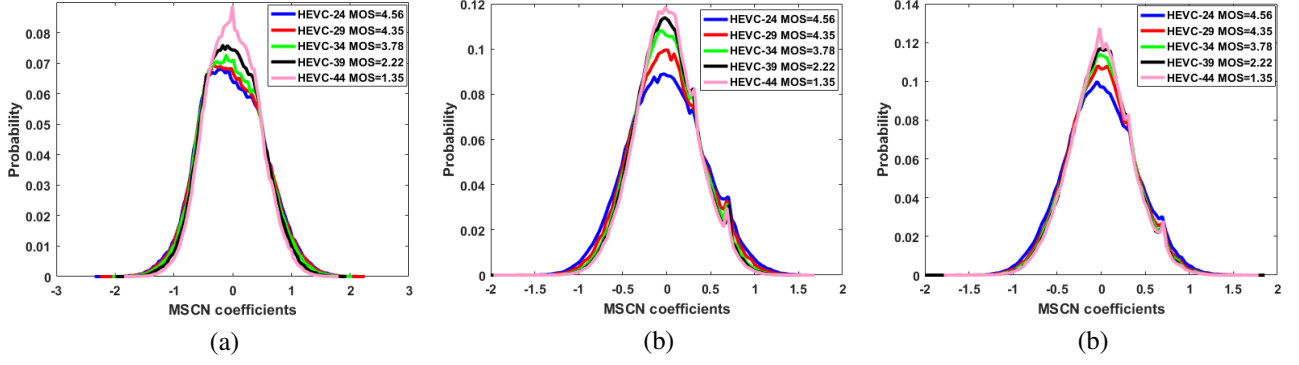
Fig. 4: MSCN coefficients for different HEVC compression levels. (a) luminance MSCN coefficients $\widehat{M_1^{0°}}$; (b) chrominance MSCN coefficients $\widehat{M_2^{0°}}$; (c) chrominance MSCN coefficients $\widehat{M_3^{0°}}$;.

of $\mathscr{C}_1^{0°}$, $\mathscr{C}_2^{0°}$ and $\mathscr{C}_3^{0°}$, respectively. Obviously, the texture information and energy mainly concentrate on the first principal component, which represents the basic texture information of the view stack. By quantitative calculation, we find the first principal component contains more than 70% energy, we thus treat it as the most important dimensionality reduced image. We define the first principal component of $\mathscr{C}_n^d$ as M_n^d, where $n = 1, 2, 3$ and $d = 0°, 45°, 90°, 135°$.

D. Feature Extraction and Quality Regression

Since the first principal component contains the basic information about each view stack, it is reasonable to extract features from the first principal component to measure the degradation of LFI spatial quality. Specifically, we first extract the PCSC from the first principal component that utilizes global naturalness and local frequency distribution characteristics to evaluate the distortion in spatial quality. In addition to spatial quality, angular consistency also affects LFI quality. Then, the TAVI is proposed to capture angular consistency distortion by computing the structural similarity between the first principal component and each view in the view stack.

1) Principal Component Spatial Characteristic (PCSC):
In general, the naturalness of an image can be effectively measured by modeling the locally mean subtracted and contrast normalized (MSCN) coefficients [29]–[31]. The MSCN has been successfully employed for image processing tasks and can be used to model the contrast-gain masking process in early human vision [31], [50]. In our model, MSCN coefficients can be calculated by:

$$\widehat{I}(x,y) = \frac{I(x,y) - \mu(x,y)}{\sigma(x,y) + 1}, \quad (7)$$

where $\widehat{I}(x,y)$ and $I(x,y)$ are the MSCN coefficients and input image (i.e. M_n^d) values at the spatial position (x,y). $\mu(x,y)$ and $\sigma(x,y)$ stand for the local mean and standard deviation in a local patch centered at (x,y). They are computed as:

$$\mu(x,y) = \sum_{k=-K}^{K} \sum_{l=-L}^{L} z_{k,l} I_{k,l}(x,y) \quad (8)$$

$$\sigma(x,y) = \sqrt{\sum_{k=-K}^{K} \sum_{l=-L}^{L} z_{k,l}(I_{k,l}(x,y) - \mu(x,y))^2}, \quad (9)$$

where $z = \{z_{k,l} | k = -K, ..., K, l = -L, ..., L\}$ denotes a 2D circularly-symmetric Gaussian weighting function with sampled out 3 standard deviations and rescaled to unit volume. In our implement, we set $K = L = 3$.

To measure the LFI spatial quality, we first consider the naturalness distribution of the principal components of luminance and chrominance (i.e. $\widehat{M_1^d}$, $\widehat{M_2^d}$ and $\widehat{M_3^d}$). Fig. 4 presents the distribution of MSCN coefficients for luminance and chrominance principal components with several HEVC compression levels. The results show that the distribution of MSCN coefficients are very indicative when the LFI suffers from artifacts. Here, the sample of LFI is selected from the Win5-LID database [8]. Since the distribution of MSCN coefficients approximates Gaussian distribution, we then utilize the zero-mean asymmetric generalized Gaussian distribution (AGGD) model to qualify the distribution of MSCN coefficients, which can fit the distribution by:

$$f(\chi; \alpha, \sigma_l^2, \sigma_r^2) = \begin{cases} \dfrac{\alpha}{(\beta_l + \beta_r)\Gamma(\frac{1}{\alpha})} exp(-(\dfrac{-x}{\beta_l})^\alpha) & \chi < 0 \\ \dfrac{\alpha}{(\beta_l + \beta_r)\Gamma(\frac{1}{\alpha})} exp(-(\dfrac{-x}{\beta_r})^\alpha) & \chi \geqslant 0, \end{cases}$$

$$(10)$$

where

$$\beta_l = \sigma_l \sqrt{\frac{\Gamma(\frac{1}{\alpha})}{\Gamma(\frac{3}{\alpha})}} \quad and \quad \beta_r = \sigma_r \sqrt{\frac{\Gamma(\frac{1}{\alpha})}{\Gamma(\frac{3}{\alpha})}}, \quad (11)$$

and α is the shape parameter controlling the shape of the statistic distribution, while σ_l and σ_r are the scale parameters of left and right sides, respectively. Moreover, we compute η as another feature by:

$$\eta = (\beta_r - \beta_l)\frac{\Gamma(\frac{2}{\alpha})}{\Gamma(\frac{1}{\alpha})} \quad (12)$$

In addition, human visual perception is also affected by the combination of luminance and chrominance channels.
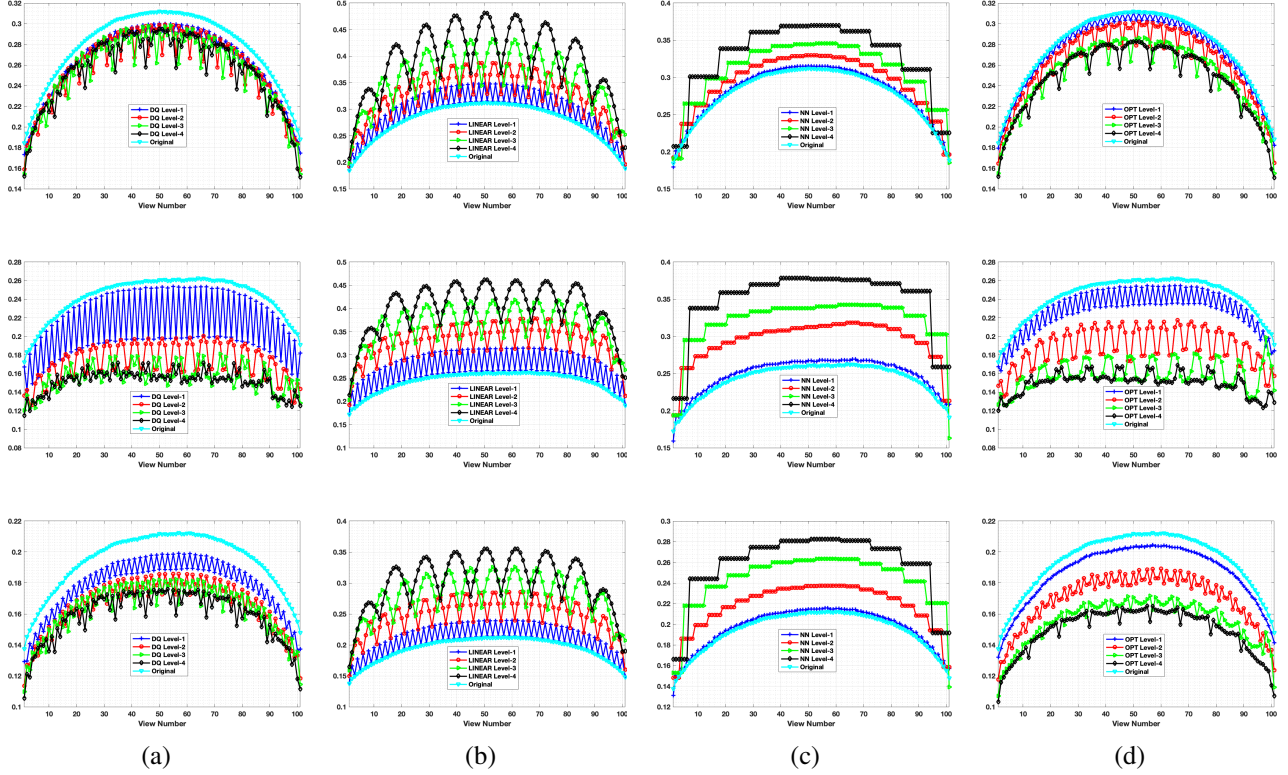
Fig. 5: Structure similarity distribution of horizontal view stack. The top row represents the $SS_1^{0^\circ}$ of luminance L channel, while the middle and bottom rows indicate the $SS_2^{0^\circ}$ and $SS_3^{0^\circ}$ of chrominance a and b channels. (a) Different DQ distortion levels; (b) Different LINEAR distortion levels; (c) Different NN distortion levels; (d) Different OPT distortion levels.

Therefore, the joint statistics of MSCN coefficients for the principal components under different channels can also be used to measure the deterioration of image quality. Therefore, we utilize multivariate generalized Gaussian distribution (MGGD) [51], [52] to fit the joint distribution, which is defined as:

$$f(\mathbf{x}|\mathbf{M}, \gamma, \varphi) = \frac{1}{|\mathbf{M}|^{\frac{1}{2}}} g_{\gamma,\varphi}\left(\mathbf{x}^T \mathbf{M}^{-1} \mathbf{x}\right), \quad (13)$$

where $\mathbf{x} \in \mathbb{R}^N$ and $\mathbf{M}$ is an $N \times N$ symmetric scatter matrix. γ and φ indicate the scale and shape parameters, respectively. $g_{\gamma,\varphi}()$ is the density generator:

$$g_{\gamma,\varphi}(\chi) = \frac{\varphi\Gamma\left(\frac{N}{2}\right)}{\left(2^{\frac{1}{\varphi}}\pi\gamma\right)^{\frac{N}{2}}\Gamma\left(\frac{N}{2\varphi}\right)} e^{-\frac{1}{2}\left(\frac{\chi}{\gamma}\right)^{\varphi}}, \quad (14)$$

where $\chi \in \mathbb{R}^+$ and Γ is the digamma function. We adopt the method proposed by Pascal *et al.* [53] to estimate the parameters of the MGGD model.

Considering that the degradation of LFI spatial quality induces the change in the local distribution of principal components. We extract the local features of principal components for each color channel. Inspired by [30], block-based discrete cosine transform (DCT) is utilized to measure the distribution of local information. Specifically, we adopt the entropy of DCT coefficients without DC value as:

$$E = -\sum_{l}^{L} \sum_{h}^{H} (p_{lh} log(p_{lh})), \quad (15)$$

where L and H represent the width and height of DCT block, respectively. c_{lh} is the DCT coefficient located in (l, h). Note that we compute the entropy from three aspects, namely the whole DCT block, three frequency bands, and three orientations of the DCT block as [30]. Therefore, F_{PSCS} is obtained by concatenating the fitting parameters of AGGD and MGGD as well as three averaged entropy features.

2) Tensor Angular Variation Index (TAVI): In addition to spatial quality, angular consistency also affects the LFI quality. Usually, angular reconstruction operations, such as interpolation, may break angular consistency. To measure the degradation of angular consistency, we propose the tensor angular variation index. Specifically, we first compute the structural similarity (SS) between each view in the view stack and its corresponding first principal component:

$$SS_n^d(i) = F_{ss}(C_n^d(i), M_n^d), \quad (16)$$

where C_n^d is the input view stack and M_n^d represents the corresponding first principal component. i indicates the angular coordinate of C. $n = 1, 2, 3$ and $d = 0°, 45°, 90°, 135°$ represent the index of three color channels and four orientations, respectively. F_{ss} is the function to calculate the structural similarity between $C_n^d(i)$ and M_n^d. In our paper, we use the SSIM [10].

flow estimation (OPT) artifacts. It can be seen that when the angular consistency is not destroyed, the distribution of structural similarity is smooth, as shown the cyan curve in Fig. 5. However, when the angular consistency is degraded by interpolation distortion, the distribution of structural similarity changes significantly. Specifically, as the angular consistency deteriorates, the variation degree in the structural similarity distribution of the LFI increases gradually. Moreover, different distortions types have different wave shapes. For example, the NN distortion is stepped and the LINEAR distortion has more peaks. These demonstrate that the structure similarity distribution is good at distinguishing various distortion types and levels.

Then, we employ a second-order polynomial to fit the SS distribution as follows:

$$SS_n^d(i) = f_1 i^2 + f_2 i + f_3, \qquad (17)$$

where i is the angular coordinate. f_1, f_2 and f_3 are fitting parameters modeling variation of angular consistency.

To further characterize the structure similarity properties, we extract several complementary features including contrast, angular second moment, entropy and inverse different moment [54] to represent the deterioration information. Specifically, the contrast is the amount of local variation presented in structure similarity. The angular second moment and inverse different moment measure the homogeneity. Thus, F_{TAVI} is obtained by concatenating the fitting parameters (i.e. f_1, f_2, f_3) and the complementary features.

3) Direction Pooling: For a LFI with an angular resolution of $S \times T$, we have S horizontal view stacks, T vertical view stacks, $S + T - 1$ main-diagonal view stacks and $S + T - 1$ secondary-diagonal view stacks. Since we extract the features of the view stack in each orientation and average the features from the stack in the same orientation, the F_d is first obtained by concatenating F_{PSCS} and F_{TAVI} in the same orientation and $d = 0°, 45°, 90°, 135°$. We then model the final features by:

$$F_{final} = w_1 F_{0°} + w_2 F_{45°} + w_3 F_{90°} + w_4 F_{135°}, \qquad (18)$$

where w_1, w_2, w_3 and w_4 indicate the corresponding weights of four orientations. In our model, we set $w_1 = w_2 = w_3 = w_4 = \frac{1}{4}$.

Finally, in this model, we train a regression model to map the final feature vector F_{final} space to quality scores. In our implementation, we adopt the well-known support vector regressor (SVR), which has been effectively applied to many image quality assessment problems [35], [36], [56]. Specifically, the LIBSVM package [57] is utilized to implement the SVR with a radial basis function (RBF) kernel.

III. EXPERIMENTAL RESULTS

To validate our proposed Tensor-NLFQ model, we conduct experiments on four publicly available databases, namely Win5-LID [8], MPI-LFA [7], SMART [5] and VALID [58].

As shown in Fig. 6(a) and Fig. 6(b), the Win5-LID database contains 6 real scenes captured by Lytro illum and 4 synthetic
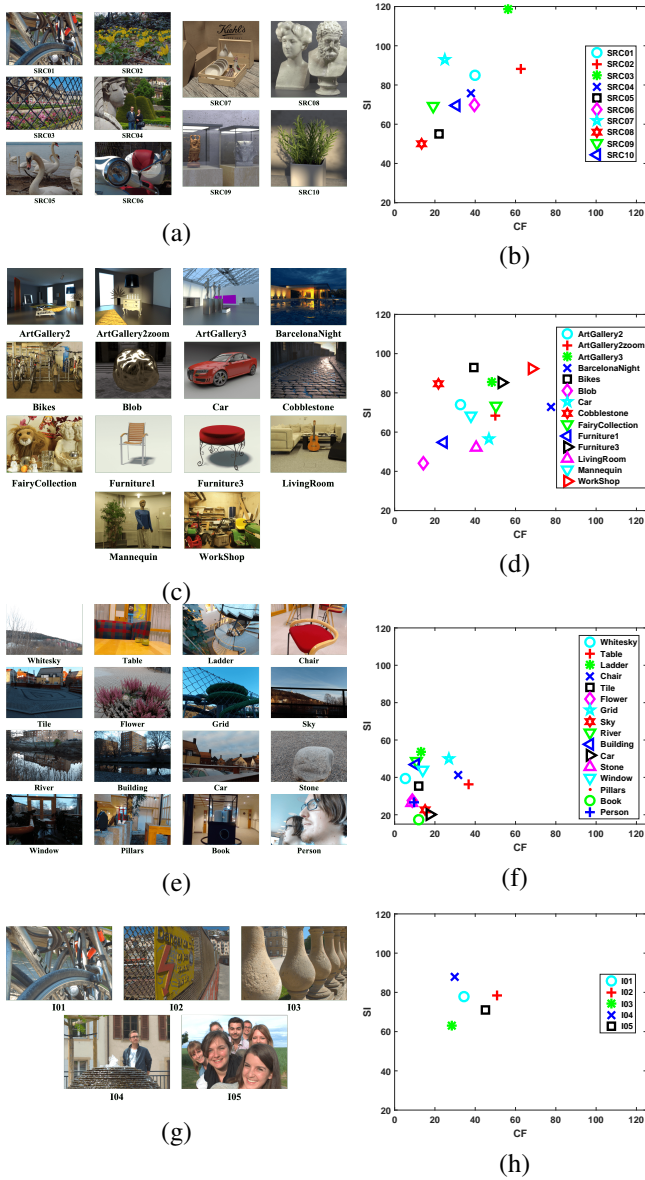

Fig. 6: Database descriptions. (a) Center view of source images for Win5-LID; (b) Distribution of SI and CF for Win5-LID; (c) Center view of source images for MPI-LFA; (d) Distribution of SI and CF for MPI-LFA; (e) Center view of source images for SMART; (f) Distribution of SI and CF for SMART; (g) Center view of source images for VALID; (h) Distribution of SI and CF for VALID.

The structure similarity distribution of LFI selected from MPI-LFA [7] is shown in Fig. 5. Since the MPI-LFI database contains only horizontal LFIs, Fig. 5 only presents the structure similarity distribution of the horizontal view stack. The top row represents the $SS_1^{0°}$ of luminance L channel, while the middle and bottom rows indicate the $SS_2^{0°}$ and $SS_3^{0°}$ of chrominance a and b channels, respectively. Fig. 5(a-d) show the structure similarity distribution of original LFI and the distribution of different distortion levels for quantized depth maps (DQ), linear interpolation (LINEAR), nearest interpolation (NN), and image warping using optical

TABLE I: Performance Comparison on Win5-LID, MPI-LFA, and SMART Databases.

Type	Metrics	Win5-LID				MPI-LFA				SMART			
		SRCC	LCC	RMSE	OR	SRCC	LCC	RMSE	OR	SRCC	LCC	RMSE	OR
2D FR	PSNR	0.6026	0.6189	0.8031	0.0045	0.8078	0.7830	1.2697	0.0060	0.7045	0.7035	1.5330	0.0195
	SSIM [10]	0.7346	0.7596	0.6650	0.0000	0.7027	0.7123	1.4327	0.0060	0.6862	0.7455	1.4378	0.0156
	MS-SSIM [11]	0.8266	0.8388	0.5566	0.0000	0.7675	0.7518	1.3461	0.0060	0.6906	0.7539	1.4171	0.0117
	FSIM [12]	0.8233	0.8318	0.5675	0.0045	0.7776	0.7679	1.3075	0.0030	0.7811	0.8139	1.2533	0.0039
	IWSSIM [13]	0.8352	0.8435	0.5492	0.0000	0.8124	0.7966	1.2340	0.0030	0.7111	0.7971	1.3024	0.0000
	IFC [17]	0.5028	0.5393	0.8611	0.0000	0.7573	0.7445	1.3629	0.0030	0.4827	0.5946	1.7343	0.0156
	VIF [18]	0.6665	0.7032	0.7270	0.0000	0.7843	0.7861	1.2618	0.0030	0.0684	0.2533	2.0867	0.0469
	NQM [19]	0.6508	0.6940	0.7362	0.0045	0.7202	0.7361	1.3817	0.0060	0.4601	0.5305	1.8285	0.0234
	VSNR [20]	0.3961	0.5050	0.8826	0.0182	0.7427	0.5787	1.6651	0.0179	0.5542	0.6289	1.6770	0.0156
	HDR-VDP2 [55]	0.5555	0.6300	0.7941	0.0045	0.8608	0.8385	1.1123	0.0000	0.1888	0.3347	2.0327	0.0625
2D NR	BRISQUE [31]	0.6687	0.7510	0.5619	0.0000	0.6724	0.7597	1.1317	0.0000	0.8239	0.8843	0.8325	0.0000
	NIQE [32]	0.2086	0.2645	0.9861	0.0045	0.0665	0.1950	2.0022	0.0327	0.1386	0.1114	2.1436	0.0547
	FRIQUEE [33]	0.6328	0.7213	0.5767	0.0000	0.6454	0.7451	1.1036	0.0000	0.7269	0.8345	0.9742	0.0000
3D FR	Chen [21]	0.5269	0.6070	0.8126	0.0091	0.7668	0.7585	1.3303	0.0030	0.6798	0.7722	1.3706	0.0078
3D NR	SINQ [35]	0.8029	0.8362	0.5124	0.0000	0.8524	0.8612	0.9939	0.0000	0.8682	0.8968	0.9653	0.0000
	BSVQE [36]	0.8179	0.8425	0.4801	0.0000	0.8570	0.8751	0.9561	0.0000	0.8449	0.8992	0.8514	0.0000
Multi-view FR	MP-PSNR Full [23]	0.5335	0.4766	0.8989	0.0000	0.7203	0.6730	1.5099	0.0089	0.8449	0.8992	0.8514	0.0000
	MP-PSNR Reduc [24]	0.5374	0.4765	0.8989	0.0000	0.7210	0.6747	1.5067	0.0089	0.6716	0.6926	1.5559	0.0117
	MW-PSNR Full [22]	0.5147	0.4758	0.8993	0.0000	0.7232	0.6770	1.5023	0.0089	0.6620	0.6505	1.6382	0.0117
	MW-PSNR Reduc [22]	0.5326	0.4766	0.8989	0.0000	0.7217	0.6757	1.5048	0.0089	0.6769	0.6903	1.5607	0.0117
	3DSwIM [25]	0.4320	0.5262	0.8695	0.0182	0.5565	0.5489	1.7063	0.0119	0.4053	0.4707	1.9032	0.0234
Multi-view NR	APT [37]	0.3058	0.4087	0.9332	0.0045	0.0710	0.0031	2.0413	0.0357	0.5105	0.5249	1.8361	0.0234
LFI FR	Fang [38]	-	-	-	-	0.7942	0.8065	1.2300	-	-	-	-	-
	Huang [39]	-	-	-	-	-	0.8954	0.9238	-	-	-	-	-
LFI RR	LF-IQM [40]	0.4503	0.4763	0.8991	0.0273	0.3364	0.4223	1.8504	0.0268	0.1222	0.2998	2.0579	0.0547
LFI NR	BELIF [41]	0.8719	0.8910	0.4294	0.0000	0.8854	0.9096	0.7877	0.0000	0.8367	0.8833	0.8347	0.0000
	Proposed Tensor-NLFQ	**0.9101**	**0.9217**	**0.3781**	**0.0000**	**0.9101**	**0.9225**	**0.7396**	**0.0000**	**0.8702**	**0.9028**	**0.8225**	**0.0000**

TABLE II: Performance Comparison on VALID Database.

Type	Metrics	VALID-8bit				VALID-10bit			
		SRCC	LCC	RMSE	OR	SRCC	LCC	RMSE	OR
2D FR	PSNR	0.9620	0.9681	0.3352	0.0000	0.9467	0.9524	0.2935	0.0000
	SSIM [10]	0.9576	0.9573	0.3868	0.0000	0.9326	0.9375	0.3348	0.0000
	MS-SSIM [11]	0.9593	0.9658	0.3473	0.0000	0.9432	0.9484	0.3051	0.0000
	FSIM [12]	0.9695	0.9798	0.2678	0.0000	-	-	-	-
	IWSSIM [13]	0.9674	0.9764	0.2892	0.0000	**0.9499**	0.9617	0.2638	0.0000
	IFC [17]	0.9693	**0.9909**	**0.1800**	0.0000	-	-	-	-
	VIF [18]	**0.9749**	0.9870	0.2150	0.0000	-	-	-	-
	NQM [19]	0.9055	0.9194	0.5266	0.0000	0.8410	0.8582	0.4940	0.0000
	VSNR [20]	0.9359	0.9324	0.4838	0.0000	-	-	-	-
	HDR-VDP2 [55]	0.9623	0.9785	0.2758	0.0000	0.9371	0.9528	0.2921	0.0000
2D NR	BRISQUE [31]	0.9222	0.9849	0.2017	0.0000	0.9027	0.9347	0.2838	0.0000
	NIQE [32]	0.8636	0.9524	0.4080	0.0000	-	-	-	-
	FRIQUEE [33]	0.9157	0.9836	0.2160	0.0000	0.8559	0.8986	0.3497	0.0000
3D FR	Chen [21]	0.9642	0.9738	0.3046	0.0000	-	-	-	-
3D NR	SINQ [35]	0.9222	0.9849	0.2070	0.0000	0.9021	0.9348	0.2722	0.0000
	BSVQE [36]	0.9222	0.9814	0.2180	0.0000	-	-	-	-
Multi-view FR	MP-PSNR Full [23]	0.9730	0.9852	0.2291	0.0000	0.3830	0.3582	0.8986	0.0000
	MP-PSNR Reduc [24]	0.9744	0.9859	0.2237	0.0000	0.3826	0.3506	0.9013	0.0000
	MW-PSNR Full [22]	0.9597	0.9677	0.3376	0.0000	0.3764	0.3556	0.8995	0.0000
	MW-PSNR Reduc [22]	0.9648	0.9751	0.2970	0.0000	0.3815	0.3563	0.8993	0.0100
	3DSwIM [25]	0.7950	0.7876	0.8248	0.0000	0.7869	0.7401	0.6472	0.0000
Multi-view NR	APT [37]	0.4699	0.6452	1.0228	0.0000	-	-	-	-
LFI RR	LF-IQM [40]	0.3934	0.5001	1.1593	0.0000	0.3679	0.3705	0.8939	0.0100
LFI NR	BELIF [41]	0.9278	0.9862	0.1680	0.0000	0.9186	0.9622	0.2387	0.0000
	Proposed Tensor-NLFQ	0.9286	0.9852	0.1825	**0.0000**	0.9367	**0.9640**	**0.2295**	**0.0000**

scenes as original images which cover various spatial perceptual information (SI) and colorfulness (CF) [59]. There exist 220 distorted LFIs by introducing 6 distortion types, including HEVC, JPEG, LN, NN and two CNN models. Moreover, more than 20 observers are invited to provide subjective ratings for the 220 distorted LFIs under double-stimulus continuous

TABLE III: Performance Comparison Between Row Method and Column Method with T-test on Win5-LID Database. The Symbol '1', '0', or '-1' Represents that the Row Method is Statistically Better, Undistinguishable, or Worse Than the Column Algorithm. Due to Space Constraints, We Use the Referenced Number Instead of The Algorithm Name.

	PSNR	[10]	[18]	[12]	[11]	[13]	[20]	[17]	[19]	[32]	[31]	[33]	[21]	[35]	[36]	[25]	[22]	[22]	[24]	[23]	[37]	[40]	[41]
Proposed	1	1	1	1	1	1	1	1	1	1	1	1	1	1	1	1	1	1	1	1	1	1	1

TABLE IV: Performance Comparison Between Row Method and Column Method with T-test on MPI-LFA Database. The Symbol '1', '0', or '-1' Represents that the Row Method is Statistically Better, Undistinguishable, or Worse Than the Column Algorithm. Due to Space Constraints, We Use the Referenced Number Instead of The Algorithm Name.

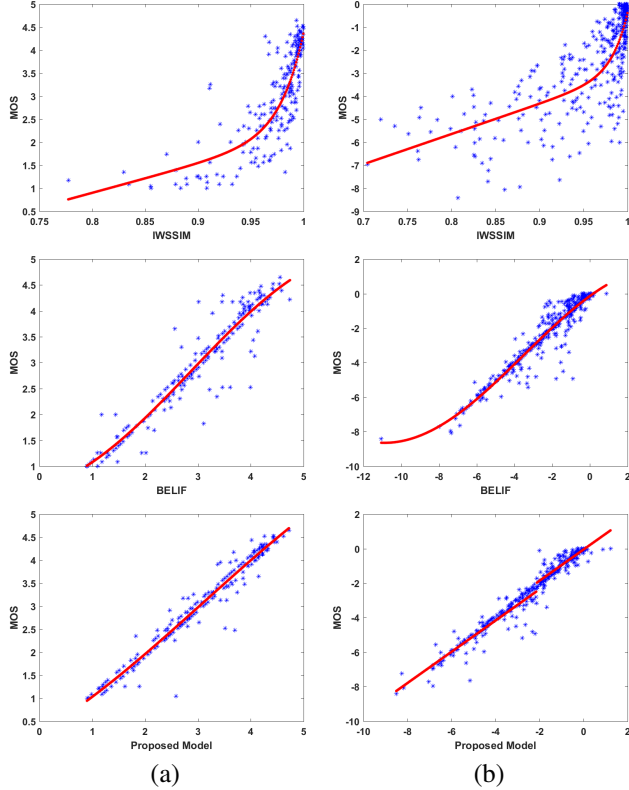|	PSNR	[10]	[18]	[12]	[11]	[13]	[20]	[17]	[19]	[32]	[31]	[33]	[21]	[35]	[36]	[25]	[22]	[22]	[24]	[23]	[37]	[40]	[41]
Proposed	1	1	1	1	1	1	1	1	1	1	1	1	1	1	1	1	1	1	1	1	1	1	1

Fig. 7: Scatter plots of predicted quality scores by three methods against the MOS values on the Win5-LID and MPI-LFA databases. The horizontal and vertical axes in each figure represent the predicted quality scores and MOS values, respectively. The red line is the fitted curve. The top, middle and bottom rows are the results of IWSSIM, BELIF and the proposed model, respectively. (a) Scatter plots on Win5-LID database; (b) Scatter plots on MPI-LFA database.

quality scale (DSCQS) on a 5-point discrete scale. Therefore, each LFI has the overall mean opinion score (MOS) value.

As we can see from Fig. 6(c) and Fig. 6(d), the MPI-LFA database consists of 14 pristine LFIs captured by the TSC system, which also cover various SI and CF. The 336 distorted LFIs are produced with 6 distortion types, i.e. HEVC, DQ, OPT, LINEAR, NN and GAUSS. In order to assess the LFI quality, the pair-wise comparison (PC) method with a two-alternative-forced-choice is carried out and just-objectionable-differences (JOD) is provided, which is similar to difference-

mean-opinion-score (DMOS) value.

Fig. 6(e) and Fig. 6(f) shows the original images and their distribution of SI and CF for the SMART database. This database is composed of 16 original LFIs and 256 distorted sequences are obtained by introducing 4 compression distortions which include HEVC Intra, JPEG, JPEG2000 and SSDC. Similarly, the PC method is exploited to collect the subjective ratings and the Bradley-Terry (BT) scores are provided.

The VALID database has 5 reference LFIs and 40 distorted LFIs under 5 compression artifacts. Fig. 6(g) and Fig. 6(h) shows the original images and the corresponding SI and CF distribution. Note that the VALID database includes both 8bit and 10bit LFIs. The comparison-based adjectival categorical judgement methodology is used to 8bit images, while double stimulus impairment scale (DSIS) is performed for 10bit images. In addition, the MOS values are provided for the LFIs.

To evaluate the model performance on these databases, we choose four evaluation criteria, including Spearman rank-order correlation coefficient (SRCC), linear correlation coefficient (LCC), root-mean-square-error (RMSE) and outlier ratio (OR). The SRCC measures the monotonicity, while LCC focuses on the linear relationship. The RMSE and OR provide the measure of prediction accuracy and consistency, respectively. Higher SRCC and LCC values as well as lower RMSE and OR values represent better performance. Before computing LCC, RMSE and OR, a nonlinear function is adopted as:

$$f(q) = \beta_1\{\frac{1}{2} - \frac{1}{1 + exp[\beta_2(q - \beta_3)]}\} + \beta_4 q + \beta_5 \quad (19)$$

where q is the output of a specific objective metric. The parameters $\beta_{1...5}$ are optimized to minimize the given goodness-of-fit measure.

Additionally, each database is randomly divided into 80% for training and the remaining 20% for testing. We perform 1000 iterations of cross validation on each database. We also provide the median SRCC, LCC, RMSE and OR values as the final measurement.

A. Comparison with Other Objective Metrics

In order to prove the effectiveness of our proposed Tensor-NLFQ model, we conduct fully experiments by using existing 2D, 3D image, multi-view and LFI quality assessment algorithms. Specifically, we compare with ten 2D FR IQA metrics [10]–[13], [17]–[20], [55], three 2D NR IQA metrics [31]–[33], one 3D FR IQA metric [21], two 3D NR IQA

TABLE V: RMSE Performance of Different Distortion Types on Win5-LID and MPI-LFA Databases.

Metrics	Win5-LID				MPI-LFA					
	HEVC	JPEG	LN	NN	HEVC	DQ	OPT	Linear	NN	GAUSS
PSNR	0.6404	0.5219	0.5233	0.3843	0.9496	1.1390	1.3430	0.9156	0.7667	0.7894
SSIM [10]	0.3808	0.5324	0.4414	0.4252	0.5578	1.5566	1.4087	1.2695	1.0692	0.4188
MS-SSIM [11]	0.2515	0.4272	0.4167	0.4170	0.4488	1.2445	1.3018	1.0766	0.7961	0.5049
FSIM [12]	0.2564	0.4377	0.4062	0.4009	0.5091	1.0886	1.2849	1.0537	0.8142	0.6747
IWSSIM [13]	0.2559	0.4133	0.3702	0.4187	0.4936	1.0900	1.1853	0.8957	0.6105	0.5343
IFC [17]	0.5396	0.6433	0.7092	0.4472	0.8244	0.8882	1.1915	0.8121	0.6229	0.9893
VIF [18]	0.2792	0.4351	0.4554	0.3712	0.4336	1.2041	1.4072	0.8385	0.7069	0.6535
NQM [19]	0.4952	0.6062	0.6228	0.5248	0.6618	1.3064	1.4238	1.1291	0.6228	0.7660
VSNR [20]	0.4460	0.4585	0.9115	0.7314	0.3249	1.7150	1.5878	1.6959	1.3126	0.6930
BRISQUE [31]	0.2695	0.2225	0.3230	0.4018	0.3468	0.7297	0.8132	0.7577	0.7733	0.4301
NIQE [32]	0.9978	0.9686	0.8986	0.7594	1.0622	1.7489	1.7262	2.0515	1.6397	1.9197
FRIQUEE [33]	0.4127	0.2273	0.3285	0.3748	0.2605	0.6906	0.8170	0.8067	0.8002	0.2551
Chen [21]	**0.2341**	0.3795	0.8978	0.6077	0.4763	1.2547	1.3122	1.0762	0.8093	0.4824
SINQ [35]	0.2373	0.2169	0.2846	0.3419	**0.1638**	0.5996	0.8109	0.6511	0.7078	0.3432
BSVQE [36]	0.2943	0.2300	0.3199	0.2628	0.3128	0.6877	0.8255	0.6571	0.4864	0.2309
MP-PSNR Full [23]	0.5357	0.5216	0.7325	0.4318	0.7634	0.9989	1.1191	0.7106	0.6670	0.9100
MP-PSNR Reduc [24]	0.4592	0.5119	0.7331	0.4255	0.9392	0.9998	1.1181	0.7179	0.6608	0.9201
MW-PSNR Full [22]	0.5857	0.5511	0.7329	0.4291	0.8729	1.0013	1.1155	0.6957	0.6426	0.7260
MW-PSNR Reduc [22]	0.4762	0.5326	0.7329	0.4313	0.8056	0.9980	1.1135	0.7130	0.6519	0.7572
3DSwIM [25]	0.9778	0.7278	0.6160	0.4536	1.9656	1.2155	1.4833	1.2782	1.2013	1.5171
APT [37]	0.9788	0.9757	0.7731	0.7196	2.2549	1.7238	1.6306	2.0857	1.6486	1.9675
LF-IQM [40]	1.0987	0.8029	0.6096	0.5409	1.8225	1.7211	1.7645	1.9623	1.5168	1.3558
BELIF [41]	0.3062	0.2013	0.3187	0.3052	0.2486	0.6513	0.8023	0.4472	0.3556	**0.1527**
Proposed Tensor-NLFQ	0.2578	**0.1902**	**0.2633**	**0.1974**	0.2030	**0.5370**	**0.7970**	**0.3555**	**0.3125**	0.1597

metrics [35], [36], five multi-view FR IQA metrics [22]–[25], one multi-view NR IQA metric [37], two FR LFI quality assessment metrics [38], [39], one RR LFI quality assessment metric [40], and one NR LFI quality assessment metric [41].

TABLE I shows the overall performance of state-of-the-art objective models on the Win5-LID, MPI-LFA and SMART databases, where bold values indicate the best performance results. As shown in this table, our proposed Tensor-NLFQ achieves superior performance compared with state-of-the-art algorithms. One possible explanation is that existing 2D and 3D IQA approaches only focus on spatial quality rather than angular consistency. Although multi-view IQA metrics consider distortion caused by angular interpolation, they aim to deal with the hole distortion caused by the synthesis. Thus, it is not possible to effectively measure LFI artifacts, such as compression distortion. The methods of Fang [38] and LFI-IQM [40] ignore the spatial texture information. Moreover, the LFI-IQM [40] is influenced by depth map estimation, while Huang [39] and BELIF [41] cannot take into account the chrominance effects and diverse directions of LFIs. Therefore, their performance is worse than that of the proposed method.

Further, we provide the performance comparison on the VALID database which includes both 8bit and 10bit LFIs. As we can see from TABLE II, the FR IQA metrics have good performance values and our proposed Tensor-NLFQ outperforms state-of-the-art NR IQA algorithms. This is because the VALID database only has 5 original LFIs, whose SI and CF distribution is relatively concentrated.

To illustrate the prediction results more clearly, the scatter plots of two existing metrics and the proposed model on the Win5-LID and MPI-LFA databases are shown in Fig. 7. Since the points of our proposed method are more centralized than that of the other metrics, the predictions of our proposed Tensor-NLFQ are more consistent with subjective quality scores.

Besides direct performance comparisons, we also quantitatively evaluate the statistical significance using the t-test [31] based on the SRCC values obtained from 1000 train-test trials. Here, the null hypothesis is that the mean correlation for row metric is equal to that for the column metric with a confidence of 95%. Specifically, a value of '0' denotes that the row metric and the column algorithm are statistically equivalent, and thus we can not reject the null hypothesis at the 95% confidence level. A value of '1' indicates that the row metric is statically superior to the column metric, while a '-1' represents that the row algorithm is statistically worse than the column algorithm. The results are shown in TABLE III and TABLE IV, which demonstrate that our proposed Tensor-NLFQ significantly outperforms state-of-the-art objective IQA algorithms.

B. Robustness Against Distortion Types

Since the Win5-LID and MPI-LFA involve various distortion types, it is interesting to know how our proposed model performs for individual distortion types. The performance results for each separate distortion type are listed in TABLE V. Due to the space constraints, we only show the results of RMSE. It can be seen that our proposed Tensor-NLFQ method outperforms existing objective metrics for most distortion types. Moreover, the proposed model achieves the best performance for typical reconstruction distortions because the reconstruction distortion mainly destroys angle consistency and usually has little influence on spatial quality. Therefore, existing IQA models are difficult to handle such distortions.

TABLE VI: Performance of Individual Color Channels on Win5-LID and MPI-LFA Databases.

Channel	Win5-LID			MPI-LFA		
	SRCC	LCC	RMSE	SRCC	LCC	RMSE
L	0.8693	0.8838	0.4438	0.8997	0.9066	0.8341
a^*	0.7574	0.7638	0.6210	0.8299	0.8468	1.0367
b^*	0.8484	0.8592	0.5038	0.8883	0.8845	0.9197
Proposed	**0.9101**	**0.9217**	**0.3781**	**0.9101**	**0.9225**	**0.7396**

TABLE VII: Performance of Four Direction View Stacks on Win5-LID Database.

Orientation	Win5-LID		
	SRCC	LCC	RMSE
Horizontal	0.8850	0.8994	0.3947
Vertical	0.8529	0.8653	0.4541
Left diagnoal	0.8795	0.8942	0.3944
Right diagnoal	0.8819	0.8894	0.4271
Proposed	**0.9101**	**0.9217**	**0.3781**

TABLE VIII: Performance of Different Structure Similarity Methods on Win5-LID and MPI-LFA Databases.

Method	Win5-LID			MPI-LFA		
	SRCC	LCC	RMSE	SRCC	LCC	RMSE
SSIM [10]	0.9101	0.9217	0.3781	0.9101	0.9225	0.7396
MS-SSIM [11]	0.9026	0.9159	0.3755	0.9305	0.9300	0.7282
FSIM [12]	0.8876	0.9087	0.4029	0.9227	0.9268	0.7743
IWSSIM [13]	0.8981	0.9149	0.3834	0.9268	0.9288	0.7368

Although HEVC compression distortion and Gaussian blur mainly cause the degradation of spatial quality, our Tensor-NLFQ is still very competitive and has a good performance. The JPEG distortion in Win5-LID is introduced based on lenslet, and it affects both spatial quality and angular consistency of LFI. The proposed method considers the effects of both two factors, it is thus not surprising that our model obtains the best performance for JPEG distorted LFIs. Overall, the proposed Tensor-NLFQ can achieve promising performance against existing objective evaluation algorithms regarding to various distortion types.

C. Validity of Individual Color Channel

Since the luminance and chrominance features of LFI are utilized in the proposed model, it is necessary to know how much contribution each color channel has. TABLE VI exhibits the performance of individual color channels on Win5-LID and MPI-LFA databases. It can be seen that the luminance channel achieves the best performance among three color channels, which proves that the luminance has the most important influence on LFI quality. Moreover, it is observed that two chrominance channels deliver good performance on two databases, which demonstrates that chrominance also has a significant impact on LFI quality.

D. Validity of Single Orientation View Stack

In the proposed Tensor-NLFQ method, we weight the extracted features of four orientation view stacks to predict the LFI overall quality. It is meaningful to verify the performance of the view stack in each orientation. Since the MPI-LFA database only includes the horizontal view stack, we present the results on the Win5-LID database, as shown in TABLE VII. We can observe that for 4D LFIs, the view stack in each direction has a good performance, which indicates that the characteristics of each orientation can reflect the LFI quality to some extent. Meanwhile, the performance of the final model with four directional feature weighting is significantly improved.

E. Different Structure Similarity Methods

In the TAVI measurement, we use SSIM [10] as an algorithm for measuring structure similarity. Except for SSIM, several variants of SSIM have been proposed, such as MS-SSIM [11], FSIM [12] and IWSSIM [13]. Therefore, we wonder how the proposed method performs when we adopt these algorithms. TABLE VIII illustrates the results of our proposed model using different structure similarity methods on Win5-LID and MPI-LFA databases, which indicates that our Tensor-NLFQ model does not rely much on specific structural similarity algorithms.

F. Validity of Individual Proposed Feature

In this section, we explore the validity of two proposed features (i.e. F_{PCSC} and F_{TAVI}) of our model. The performance values of these two features are shown in TABLE IX. It can be seen that F_{PCSC} has a good performance on both databases due to the effectiveness of measuring spatial quality, especially on the MPI-LFA database. The reason may be that some interpolation operations in the MPI-LFA database can also cause the degradation of spatial quality. Therefore, in addition to capture the deterioration of spatial quality, F_{PCSC} can also measure a certain degree of angular distortion. Furthermore, F_{TAVI} delivers the slightly lower performance on the MPI-LFA database. Since the MPI-LFA database contains many angular distorted LFIs with low distortion levels and the quality difference is small, human is insensitive to these sequences. However, the proposed F_{TAVI} can capture the degradation of angular consistency effectively. This phenomenon can be shown in Fig. 5, where the curve of distortion sequences are significantly different. Overall, the results validate our proposed features and the performance is improved after the feature combination.

G. Model Generality and Time Complexity

To validate the model generality, we choose the same distortion in the MPI-LFA and Win5-LID databases to conduct experiments. Specifically, we train the proposed Tensor-NLFQ on the Win5-LID database, and then test it on the LFIs with the same distortion in the MPI-LFA database. The results are shown in TABLE X. We can observe that the proposed model is independent for the adopted database.

In addition, we compare the proposed Tensor-NLFQ method with LF-IQM [40] for computational complexity on the Win5-LID database. As shown in TABLE XI, our proposed Tensor-NLFQ is demonstrated to have lower computation time compared to LF-IQM. The reason may be that different from

TABLE IX: Performance of Proposed Quality Components on Win5-LID and MPI-LFA Databases.

Features	Win5-LID			MPI-LFA		
	SRCC	LCC	RMSE	SRCC	LCC	RMSE
F_{PCSC}	0.8001	0.8188	0.5821	0.8749	0.8815	0.8345
F_{TAVI}	0.8318	0.8521	0.4648	0.7912	0.7964	1.1669
Proposed	**0.9101**	**0.9217**	**0.3781**	**0.9101**	**0.9225**	**0.7396**

TABLE X: Cross Validation Results. We Train Our Proposed Model on Win5-LID and Test on MPI-LFA.

	SRCC	LCC	RMSE
Proposed	0.8469	0.8192	0.3282

TABLE XI: Performance Comparison of The Computation Time on Win5-LID Database.

Methods	LF-IQM [40]	Proposed Tensor-NLFQ
Total time (s)	1168.7276	865.0019

conventional LFI quality assessment metrics, our proposed approach relieves the complex computation for estimating depth maps.

IV. CONCLUSION

In this paper, we present a novel Tensor oriented No-reference Light Field image Quality evaluator (Tensor-NLFQ). The main contributions of this work are summarized as: 1) According to the existing research and our previous work, color information has a significant impact on the perceived LFI quality. We thus introduce luminance and chrominance information in our proposed model. 2) Since the LFI can be regarded as a high-dimensional tensor signal, we exploit the tensor decomposition to extract the principal components of LFI, which can effectively reflect the LFI quality. 3) The angular consistency of diverse directions is considered in the proposed method, including horizontal, diagonal, vertical and right diagonal orientations. 4) As the LFI quality is affected by both spatial quality and angular consistency, we propose principal component spatial characteristic and tensor angular variation index to measure the degradation of spatial quality and angular consistency, respectively. 5) We conduct extensive experiments to compare the proposed Tensor-NLFQ with existing 2D, 3D image, multi-view and LFI quality assessment algorithms. The results demonstrate that our approach outperforms state-of-the-art metrics and can handle the typical distortions of LFI.

In the future work, we will extend the proposed model to light field video quality assessment. Moreover, how to apply our proposed method to the optimization of existing image compression and reconstruction algorithms could also be further explored.

REFERENCES

[1] G. Wu, B. Masia, A. Jarabo, Y. Zhang, L. Wang, Q. Dai, T. Chai, and Y. Liu, "Light field image processing: An overview," *IEEE Journal of Selected Topics in Signal Processing*, vol. 11, no. 7, pp. 926–954, 2017.

[2] M. Levoy and P. Hanrahan, "Light field rendering," in *Proceedings of the 23rd annual conference on Computer graphics and interactive techniques*. ACM, 1996, pp. 31–42.

[3] S. J. Gortler, R. Grzeszczuk, R. Szeliski, and M. F. Cohen, "The lumigraph," in *Proceedings of the 23rd annual conference on Computer graphics and interactive techniques*. ACM, 1996, pp. 43–54.

[4] Lytro, http://www.lytro.com, 2017.[Online].

[5] P. Paudyal, F. Battisti, M. Sjöström, R. Olsson, and M. Carli, "Towards the perceptual quality evaluation of compressed light field images," *IEEE Transactions on Broadcasting*, vol. 63, no. 3, pp. 507–522, 2017.

[6] I. Viola, M. Rerabek, and T. Ebrahimi, "Comparison and evaluation of light field image coding approaches," *IEEE Journal of selected topics in signal processing*, vol. 11, no. EPFL-ARTICLE-230995, 2017.

[7] V. K. Adhikarla, M. Vinkler, D. Sumin, R. K. Mantiuk, K. Myszkowski, H.-P. Seidel, and P. Didyk, "Towards a quality metric for dense light fields," in *Computer Vision and Pattern Recognition (CVPR), 2017 IEEE Conference on*. IEEE, 2017, pp. 3720–3729.

[8] L. Shi, S. Zhao, W. Zhou, and Z. Chen, "Perceptual evaluation of light field image," in *2018 25th IEEE International Conference on Image Processing (ICIP)*, Oct 2018, pp. 41–45.

[9] P. A. Kara, P. T. Kovacs, S. Vagharshakyan, M. G. Martini, A. Barsi, T. Balogh, A. Chuchvara, and A. Chehaibi, "The effect of light field reconstruction and angular resolution reduction on the quality of experience," in *Signal-Image Technology & Internet-Based Systems (SITIS), 2016 12th International Conference on*. IEEE, 2016, pp. 781–786.

[10] Z. Wang, A. C. Bovik, H. R. Sheikh, and E. P. Simoncelli, "Image quality assessment: from error visibility to structural similarity," *IEEE Transactions on image processing*, vol. 13, no. 4, pp. 600–612, 2004.

[11] Z. Wang, E. P. Simoncelli, and A. C. Bovik, "Multiscale structural similarity for image quality assessment," in *Signals, Systems and Computers, 2004. Conference Record of the Thirty-Seventh Asilomar Conference on*, vol. 2. Ieee, 2003, pp. 1398–1402.

[12] L. Zhang, L. Zhang, X. Mou, and D. Zhang, "FSIM: A feature similarity index for image quality assessment," *IEEE Transactions on Image Processing*, vol. 20, no. 8, pp. 2378–2386, 2011.

[13] Z. Wang and Q. Li, "Information content weighting for perceptual image quality assessment," *IEEE Transactions on Image Processing*, vol. 20, no. 5, pp. 1185–1198, 2011.

[14] J. Wu, W. Lin, G. Shi, and A. Liu, "Perceptual quality metric with internal generative mechanism," *IEEE Transactions on Image Processing*, vol. 22, no. 1, pp. 43–54, 2013.

[15] L. Zhang, Y. Shen, and H. Li, "VSI: A visual saliency-induced index for perceptual image quality assessment," *IEEE Transactions on Image Processing*, vol. 23, no. 10, pp. 4270–4281, 2014.

[16] W. Xue, L. Zhang, X. Mou, and A. C. Bovik, "Gradient magnitude similarity deviation: A highly efficient perceptual image quality index," *IEEE Transactions on Image Processing*, vol. 23, no. 2, pp. 684–695, 2014.

[17] H. R. Sheikh, A. C. Bovik, and G. De Veciana, "An information fidelity criterion for image quality assessment using natural scene statistics," *IEEE Transactions on image processing*, vol. 14, no. 12, pp. 2117–2128, 2005.

[18] H. R. Sheikh and A. C. Bovik, "Image information and visual quality," *IEEE Transactions on image processing*, vol. 15, no. 2, pp. 430–444, 2006.

[19] N. Damera-Venkata, T. D. Kite, W. S. Geisler, B. L. Evans, and A. C. Bovik, "Image quality assessment based on a degradation model," *IEEE Transactions on image processing*, vol. 9, no. 4, pp. 636–650, 2000.

[20] D. M. Chandler and S. S. Hemami, "VSNR: A wavelet-based visual signal-to-noise ratio for natural images," *IEEE Transactions on image processing*, vol. 16, no. 9, pp. 2284–2298, 2007.

[21] M.-J. Chen, C.-C. Su, D.-K. Kwon, L. K. Cormack, and A. C. Bovik, "Full-reference quality assessment of stereopairs accounting for rivalry," *Signal Processing: Image Communication*, vol. 28, no. 9, pp. 1143–1155, 2013.

[22] D. Sandić-Stanković, D. Kukolj, and P. Le Callet, "DIBR synthesized image quality assessment based on morphological wavelets," in *Seventh International Workshop on Quality of Multimedia Experience (QoMEX)*. IEEE, 2015, pp. 1–6.

[23] D. Sandic-Stankovic, D. Kukolj, and P. Le Callet, "DIBR synthesized image quality assessment based on morphological pyramids, 3DTV-CON immersive and interactive 3D media experience over networks," *Lisbon, July*, 2015.

[24] D. Sandić-Stanković, D. Kukolj, and P. Le Callet, "Multi-scale synthesized view assessment based on morphological pyramids," *Journal of Electrical Engineering*, vol. 67, no. 1, pp. 3–11, 2016.

[25] F. Battisti, E. Bosc, M. Carli, P. Le Callet, and S. Perugia, "Objective image quality assessment of 3D synthesized views," *Signal Processing: Image Communication*, vol. 30, pp. 78–88, 2015.

[26] Z. Wang and E. P. Simoncelli, "Reduced-reference image quality assessment using a wavelet-domain natural image statistic model," in *Human Vision and Electronic Imaging X*, vol. 5666. International Society for Optics and Photonics, 2005, pp. 149–160.

[27] Z. Wang and A. C. Bovik, "Reduced-and no-reference image quality assessment," *IEEE Signal Processing Magazine*, vol. 28, no. 6, pp. 29–40, 2011.

[28] A. Rehman and Z. Wang, "Reduced-reference image quality assessment by structural similarity estimation," *IEEE Transactions on Image Processing*, vol. 21, no. 8, pp. 3378–3389, 2012.

[29] A. K. Moorthy and A. C. Bovik, "Blind image quality assessment: From natural scene statistics to perceptual quality," *IEEE Transactions on Image Processing*, vol. 20, no. 12, pp. 3350–3364, 2011.

[30] M. A. Saad, A. C. Bovik, and C. Charrier, "Blind image quality assessment: A natural scene statistics approach in the DCT domain," *IEEE Transactions on Image Processing*, vol. 21, no. 8, pp. 3339–3352, 2012.

[31] A. Mittal, A. K. Moorthy, and A. C. Bovik, "No-reference image quality assessment in the spatial domain," *IEEE Transactions on Image Processing*, vol. 21, no. 12, pp. 4695–4708, 2012.

[32] A. Mittal, R. Soundararajan, and A. C. Bovik, "Making a "completely blind" image quality analyzer," *IEEE Signal Processing Letters*, vol. 20, no. 3, pp. 209–212, 2012.

[33] D. Ghadiyaram and A. C. Bovik, "Perceptual quality prediction on authentically distorted images using a bag of features approach," *Journal of vision*, vol. 17, no. 1, pp. 32–32, 2017.

[34] M.-J. Chen, L. K. Cormack, and A. C. Bovik, "No-reference quality assessment of natural stereopairs," *IEEE Transactions on Image Processing*, vol. 22, no. 9, pp. 3379–3391, 2013.

[35] L. Liu, B. Liu, C.-C. Su, H. Huang, and A. C. Bovik, "Binocular spatial activity and reverse saliency driven no-reference stereopair quality assessment," *Signal Processing: Image Communication*, vol. 58, pp. 287–299, 2017.

[36] Z. Chen, W. Zhou, and W. Li, "Blind stereoscopic video quality assessment: From depth perception to overall experience," *IEEE Transactions on Image Processing*, vol. 27, no. 2, pp. 721–734, 2018.

[37] K. Gu, V. Jakhetiya, J.-F. Qiao, X. Li, W. Lin, and D. Thalmann, "Model-based referenceless quality metric of 3D synthesized images using local image description," *IEEE Transactions on Image Processing*, vol. 27, no. 1, pp. 394–405, 2018.

[38] Y. Fang, K. Wei, J. Hou, W. Wen, and N. Imamoglu, "Light filed image quality assessment by local and global features of epipolar plane image," in *2018 IEEE Fourth International Conference on Multimedia Big Data (BigMM)*. IEEE, 2018, pp. 1–6.

[39] Z. Huang, M. Yu, H. Xu, Y. Song, H. Jiang, and G. Jiang, "New quality assessment method for dense light fields," in *Optoelectronic Imaging and Multimedia Technology V*, vol. 10817. International Society for Optics and Photonics, 2018, p. 1081717.

[40] P. Paudyal, F. Battisti, and M. Carli, "Reduced reference quality assessment of light field images," *IEEE Transactions on Broadcasting*, vol. 65, no. 1, pp. 152–165, 2019.

[41] L. Shi, S. Zhao, and Z. Chen, "BELIF: Blind quality evaluator of light field image with tensor structure variation index," in *2019 26th IEEE International Conference on Image Processing (ICIP)*, 2019, Accepted.

[42] T. G. Kolda and B. W. Bader, "Tensor decompositions and applications," *SIAM review*, vol. 51, no. 3, pp. 455–500, 2009.

[43] W. Lin and C.-C. J. Kuo, "Perceptual visual quality metrics: A survey," *Journal of Visual Communication and Image Representation*, vol. 22, no. 4, pp. 297–312, 2011.

[44] D. Lee and K. N. Plataniotis, "Towards a full-reference quality assessment for color images using directional statistics," *IEEE Transactions on image processing*, vol. 24, no. 11, pp. 3950–3965, 2015.

[45] D. Temel and G. AlRegib, "CSV: Image quality assessment based on color, structure, and visual system," *Signal Processing: Image Communication*, vol. 48, pp. 92–103, 2016.

[46] D. Lee and K. N. Plataniotis, "Toward a no-reference image quality assessment using statistics of perceptual color descriptors," *IEEE Transactions on Image Processing*, vol. 25, no. 8, pp. 3875–3889, 2016.

[47] U. Rajashekar, Z. Wang, and E. P. Simoncelli, "Perceptual quality assessment of color images using adaptive signal representation," in *Human Vision and Electronic Imaging XV*, vol. 7527. International Society for Optics and Photonics, 2010, p. 75271L.

[48] M. Lee and C.-H. Choi, "Incremental n-mode SVD for large-scale multilinear generative models," *IEEE Transactions on Image Processing*, vol. 23, no. 10, pp. 4255–4269, 2014.

[49] B. W. Bader, T. G. Kolda *et al.*, "Matlab tensor toolbox version 2.6," Available online, February 2015. [Online]. Available: http://www.sandia.gov/~tgkolda/TensorToolbox/

[50] M. Carandini, D. J. Heeger, and J. A. Movshon, "Linearity and normalization in simple cells of the macaque primary visual cortex," *Journal of Neuroscience*, vol. 17, no. 21, pp. 8621–8644, 1997.

[51] C.-C. Su, L. K. Cormack, and A. C. Bovik, "Bivariate statistical modeling of color and range in natural scenes," in *Human Vision and Electronic Imaging XIX*, vol. 9014. International Society for Optics and Photonics, 2014, p. 90141G.

[52] Z. Sinno, C. Caramanis, and A. C. Bovik, "Towards a closed form second-order natural scene statistics model," *IEEE Transactions on Image Processing*, vol. 27, no. 7, pp. 3194–3209, 2018.

[53] F. Pascal, L. Bombrun, J.-Y. Tourneret, and Y. Berthoumieu, "Parameter estimation for multivariate generalized Gaussian distributions," *IEEE Transactions on Signal Processing*, vol. 61, no. 23, pp. 5960–5971, 2013.

[54] H. G. Kim, Y. E. Chung, Y. H. Lee, J.-Y. Choi, M.-S. Park, M.-J. Kim, and K. W. Kim, "Quantitative analysis of the effect of iterative reconstruction using a phantom: determining the appropriate blending percentage," *Yonsei medical journal*, vol. 56, no. 1, pp. 253–261, 2015.

[55] R. Mantiuk, K. J. Kim, A. G. Rempel, and W. Heidrich, "HDR-VDP-2: a calibrated visual metric for visibility and quality predictions in all luminance conditions," in *ACM Transactions on Graphics (TOG)*, vol. 30, no. 4. ACM, 2011, p. 40.

[56] W. Zhou, N. Liao, Z. Chen, and W. Li, "3D-HEVC visual quality assessment: Database and bitstream model," in *Eighth International Conference on Quality of Multimedia Experience (QoMEX)*. IEEE, 2016, pp. 1–6.

[57] C.-C. Chang and C.-J. Lin, "LIBSVM: a library for support vector machines," *ACM Transactions on intelligent systems and technology (TIST)*, vol. 2, no. 3, p. 27, 2011.

[58] I. Viola and T. Ebrahimi, "VALID: Visual quality assessment for light field images dataset," in *10th International Conference on Quality of Multimedia Experience (QoMEX)*, no. CONF, 2018.

[59] P. ITU-T RECOMMENDATION, "Subjective video quality assessment methods for multimedia applications," *International telecommunication union*, 1999.